Quasistatic behavior and force transmission in packing of irregular polyhedral particles

Emilien Azéma, Farhang Radjai, Gilles Saussine

Quasistatic behavior and force transmission in packing of irregular polyhedral particles

Emilien Azéma*, Farhang. Radjai* and Gilles Saussine†

*LMGC, Université Montpellier 2, 34080 Montpellier cedex 05, France
†Innovation and Research Departement of SNCF, 45 rue de Londres, 75379 Paris Cedex 08, France

Abstract. Dense packings composed of irregular polyhedral particles are investigated by numerical simulations under quasistatic triaxial compression. The Contact Dynamics method is used for this investigation with 40 000 particles. The effect of particle shape is analyzed by comparing this packing with a packing of similar particle size distribution but with spherical particles. We analyze the origin of the higher shear strength of the polyhedra packing by considering various anisotropy parameters characterizing the microstructure and force transmission. Remarkably, we find that the polyhedra packing has a lower fabric anisotropy in terms of branch vectors (joining the particle centers) than the sphere packing. In contrast, the polyhedra packing shows a much higher force anisotropy which is at the origin of its higher shear strength. The force anisotropy in the polyhedra packing is shown to be related to the formation of face-face contacts. In particular, most face-face contacts belong to strong force chains along the major principal stress direction whereas vertex-face and edge-edge contacts are correlated with weak forces and oriented on average along the minor principal stress direction in steady shearing.

Keywords: Granular materials, contact dynamics method, shear strength, anisotropy
PACS: 45.70.-n,61.43.-j,83.80.Fg,7.57.Gc

INTRODUCTION

During the last two decades, granular media composed of circular particles (in 2D) and spheres (in 3D) have been a subject of systematic research. In particular, various microscopic features such as fabric anisotropy [1], force transmission [2, 3, 4, 5, 6] and friction mobilization [7] have been analyzed numerically and experimentally. Hence, an emerging issue today is how robust these findings are with respect to particle properties such as shape and size distribution [8, 9, 10].

In this paper, we study numerically granular materials composed of polyhedral particles. We use the contact dynamics method to simulate the slow shear of these materials in comparison to sphere packings with similar particle size distribution. The facetted shapes give rise to a rich microstructure where the particles touch at their faces, edges and vertices. We analyze the fabric and force anisotropies and their link with the stress-strain behavior. We show that face-face contacts play a major role in force transmission and statics of polyhedra by accommodating long force chains that are basically unstable in a packing composed of spheres.

NUMERICAL PROCEDURES

The simulations were carried out by means of the contact dynamics (CD) method with irregular polyhedra particles [11, 12]. We used LMGC90 which is a multipurpose software developed in our laboratory, capable of modeling a collection of deformable or undeformable particles of various shapes by different algorithms [13].

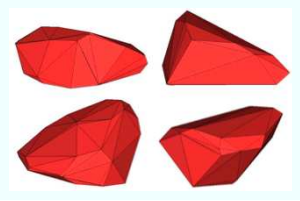

FIGURE 1. Examples of polyhedra used in the simulations.

We generate two numerical samples. The first sample (S1) is composed of 36933 polyhedra. The particle shapes are taken from a library of 1000 digitalized ballast grains provided by the French Railway Company SNCF. Fig. 1 shows several examples of the polyhedral particles used in the simulations. We used the following size distribution: 50% of diameter $d_{min} = 2.5$ cm, 34% of diameter 3.75 cm, 16% of diameter $d_{max} = 5$ cm, where d_{min} is defined as two times the largest distance between the barycenter and the vertices of the particle. The second sample (S2) is composed of 19998 spheres with exactly the same size distribution as in S1. Fig. 2 shows a snapshot of the sample S1 in equilibrium state after deposition and isotropic compression under a constant stress of $\sigma_0 = 10^4$ Pa in a rectangular box at zero gravity.

The coefficient of friction is 0.5 between the particles and 0 with the walls. The initial value of the solid fraction is $\rho \simeq 0.6$ in both samples. Both samples have a nearly

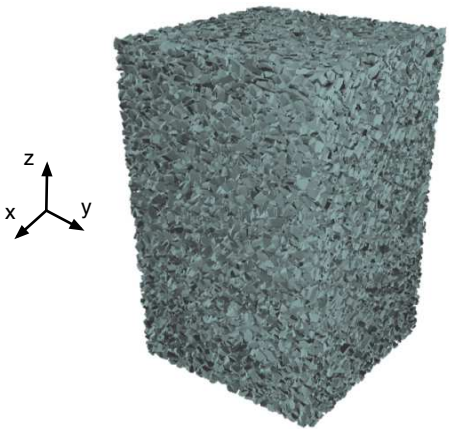

FIGURE 2. A snapshot of the packing S1 (polyhedra). The walls are not shown.

square bottom of side such that $L \approx l$ and an aspect ratio $H/L \simeq 2$, where H is the height. The isotropic samples were subjected to vertical compression by downward displacement of the top wall at a constant velocity of 1 cm/s for a constant confining stress σ_0 acting on the lateral walls.

SHEAR STRENGTH

In this section, we compare the stress-strain behavior between the packings of polyhedra (packing S1) and spheres (packing S2). For the estimation of the stress tensor, we use the internal moment tensor $\boldsymbol{M}^i$ of each particle i defined by [14]:

$$M^i_{\alpha\beta} = \sum_{c\in i} f^c_\alpha r^c_\beta, \qquad (1)$$

where f^c_α is the α component of the force exerted on particle i at the contact c, r^c_β is the β component of the position vector of the same contact c, and the summation runs over all contact neighbors of particle i.

It can be shown that the internal moment of a collection of rigid particles is the sum of the internal moments of individual particles [14]. The stress tensor $\boldsymbol{\sigma}$ for a packing of volume V is simply given by

$$\boldsymbol{\sigma} = \frac{1}{V}\sum_{i\in V} \boldsymbol{M}^i = \frac{1}{V}\sum_{c\in V} f^c_\alpha \ell^c_\beta, \qquad (2)$$

where $\boldsymbol{\ell}^c$ is the branch vector joining the centers of the two touching particles at the contact c.

Under triaxial conditions with vertical compression, we have $\sigma_1 \geq \sigma_2 = \sigma_3$, where the σ_α are the stress principal values. We extract the mean stress $p = (\sigma_1 + \sigma_2 + \sigma_3)/3$, and the stress deviator $q = (\sigma_1 - \sigma_3)/3$. For our system of perfectly rigid particles, the stress state is characterized by the mean stress p and the normalized shear stress q/p.

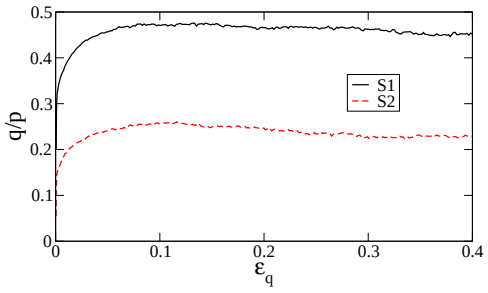

FIGURE 3. The normalized shear stress q/p as a function of shear strain ε_q for the polyhedra packing S1 and sphere packing S2.

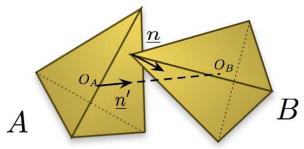

FIGURE 4. Geometry of a contact between two polyhedra.

The cumulative strain components ε_α are defined by

$$\varepsilon_1 = \int_{H_0}^{H} \frac{dH'}{H'}, \varepsilon_2 = \int_{L_0}^{L} \frac{dL'}{L'}, \varepsilon_3 = \int_{l_0}^{l} \frac{dl'}{l'}, \qquad (3)$$

where H_0, l_0 and L_0 are the initial height, width and length of the simulation box, respectively, and $\Delta H = H_0 - H$, $\Delta l = l_0 - l$ and $\Delta L = L_0 - L$ are the corresponding cumulative displacements. The cumulative shear strain is defined by $\varepsilon_q \equiv \varepsilon_1 - \varepsilon_3$.

Figure 3 displays the evolution of q/p for the packings S1 and S2 as a function of ε_q. For both packings, we observe a classical behavior characterized by a hardening behavior followed by (slight) softening and a stress plateau. The higher level of q/p for the polyhedra packing reflects the organization of the microstructure and the features of force transmission that we analyze below.

GEOMETRICAL ANISOTROPY

For the analyses that will be discussed below, we introduce the local frame $(\boldsymbol{n}', \boldsymbol{t}')$ where $\boldsymbol{n}'$ is the unit vector along the branch $\boldsymbol{l}$ and $\boldsymbol{t}'$ is an orthonormal unit vector ; figure 4. We set

$$\boldsymbol{\ell} = \ell \boldsymbol{n}', \qquad (4)$$

where ℓ is the length of the branch vector.

We define the angular averages associated with the branch vectors $\boldsymbol{\ell}$. Let $\mathscr{A}(\Omega)$ be the set of branch vectors

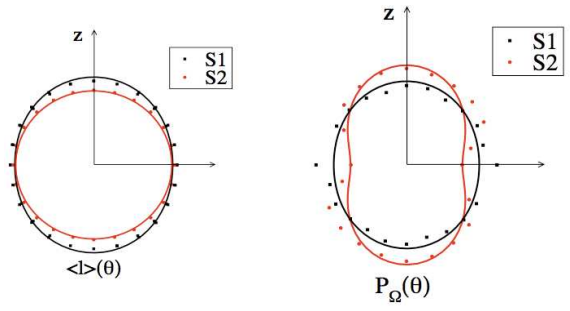

FIGURE 5. Polar representation of the probability density function P_Ω and $\langle \ell(\Omega) \rangle$ for the samples S1 and S2 in the residual state.

pointing in the direction $\Omega \equiv (\theta, \phi)$ up to a solid angle $d\Omega$ and $N_c(\Omega)$ its cardinal. The angular averages are defined as follows:

$$P_\Omega(\Omega) = \frac{N_c(\Omega)}{N_c}, \quad \langle \ell \rangle(\Omega) = \frac{1}{N_c(\Omega)} \sum_{c \in \mathscr{A}(\Omega)} \ell^c, \qquad (5)$$

where N_c is the total number of contacts, and ℓ^c,is the actual values of branch vector length, for contact c, respectively.

Under the axisymmetric conditions of our simulations, these two functions are independent of ϕ. Fig. 5 displays a polar representation of these functions in the θ-plane for polyhedra (S1) and spheres (S2) at $\varepsilon_q = 0.3$. We observe an anisotropic behavior of the unit inter-center vector $P_\Omega(\theta)$ in both cases. A weak anisotropy of branch vector can be seen for S1. The magnitude of anisotropy is larger for spheres compared to polyhedra except for $\langle \ell \rangle(\theta)$ which is weakly anisotropic for polyhedra.

The simple shapes of the above functions can be approximated by harmonic approximation. Considering only the functions compatible with the symmetries of the problem (independent with respect to ϕ and π-periodic as a function of θ) we have

$$P_\Omega(\theta) = \frac{1}{4\pi}\{\, 1 + a\,[3\cos^2\theta - 1]\,\}, \qquad (6)$$

$$\langle \ell \rangle(\theta) = \ell_0\{\, 1 + a_l\,[3\cos^2\theta - 1]\,\} \qquad (7)$$

where a, a_l are the anisotropy parameters, ℓ_0 is the mean branch vector length. The probability density function $P_\Omega(\theta)$ is normalized to 1. The harmonic fits are shown in figure 5 for the two functions in the critical state.

The evolution of the anisotropies with ε_q are displayed in Fig. 6 for S1 and S2. We see that a is systematically larger for spheres than for polyhedra. The branch vector length anisotropy a_l is negligible for spheres. The low anisotropy of the polyhedra packing results from a particular organization of the force network in correlation with the orientations of each contacts (edge-to-face, vertex-to-edge...) in the packing [10, 15].

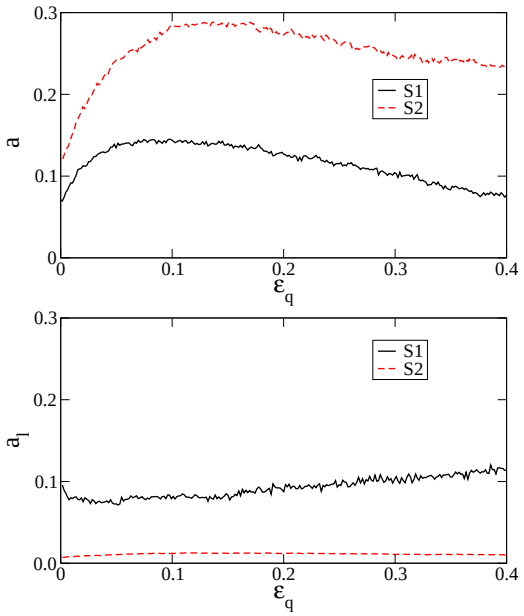

FIGURE 6. Evolution of anisotropies a, a_l with ε_q for packings S1 and S2.

FORCE ANISOTROPY

We consider the components of the contact force by

$$\boldsymbol{f} = f_{n'}\boldsymbol{n'} + f_{t'}\boldsymbol{t'}. \qquad (8)$$

We refer to $f_{n'}$ and $f_{t'}$ as *radial* and *orthoradial* components of the contact force. As the angular orientation of the branch vector, we distinguish the angular distributions of radial forces $\langle f_{n'} \rangle(\Omega)$ and orthoradial forces $\langle f_{t'} \rangle(\Omega)$. These two functions can be expanded on a base of spherical harmonics. At leading order, we have [8, 15]

$$\begin{cases} \langle f_{n'} \rangle(\theta) &= f_0\{\, 1 + a_{n'}\,[3\cos^2\theta - 1]\,\}, \\ \langle f_{t'} \rangle(\theta) &= f_0\, a_{t'}\, \sin 2\theta, \end{cases} \qquad (9)$$

where $a_{n'}$ and $a_{t'}$ are the anisotropy parameters, and f_0 the mean force. The anisotropies $a_{n'}$ and $a_{t'}$ are plotted in figure 7 as a function of ε_q. The radial force anisotropy $a_{n'}$ increases as the fabric anisotropy, and tends to a plateau. But, in contrast to fabric anisotropy, its value is higher for polyhedra than for spheres. This means that the large force anisotropy is correlated with particle shape rather than with fabric anisotropy. The orthoradial force anisotropy $a_{t'}$ has a similar behavior except that it takes considerably higher values in the case of polyhedra compared to spheres due to large friction developed by face to face contacts [10, 15].

The anisotropies a, a_l, $a_{n'}$ and $a_{t'}$ are interesting descriptors of granular microstructure and force transmission as they underlie the shear stress. Indeed, it can be shown that the general expression of the stress tensor Eq.

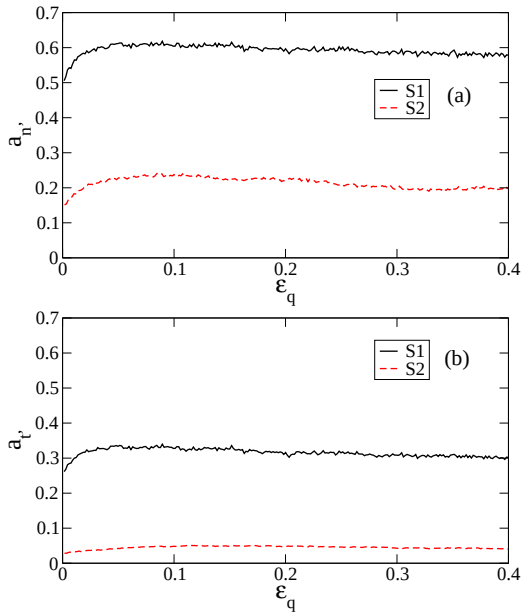

FIGURE 7. Evolution of anisotropies $a_{n'}$, $a_{t'}$ with ε_q for packings S1 and S2.

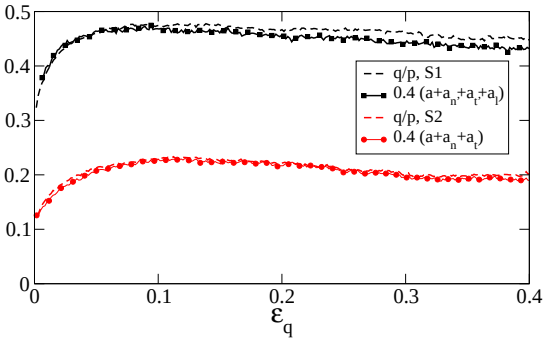

FIGURE 8. The normalized shear stress q/p as a function of shear strain ε_q for the packings S1 and S2 both from direct simulation data and theoretical prediction of Eq. (10).

(2) under some approximations leads to the following simple “stress-force-fabric" relation [1, 8, 15]:

$$\frac{q}{p} \simeq \frac{2}{5}\,(a + a_l + a_{n'} + a_{t'}), \qquad (10)$$

As we see in Fig. 8, our simulation data are in quantitative agreement with this relation both for spheres and polyhedra, all along the shear. A remarkable consequence of Eq. (10) is to reveal that the fabric anisotropy provides a major contribution to shear stress in the sphere packing whereas the force anisotropies are more important for shear stress in the polyhedra packing.

CONCLUSION

The objective of this paper was to isolate the effect of particle shape with respect to shear strength in 3D granular media by comparing two similar packings with different particle shapes. A novel finding of this work is that the origin of enhanced shear strength in a polyhedra packing compared to a sphere packing lies in force anisotropy induced by particle shape. The fabric anisotropy associated with the network of branch vectors is lower in the polyhedra packing. In other words, the force anisotropy, partially underlying shear strength, is mainly controlled by the fabric anisotropy in a sphere packing. This mechanism breaks down to some extent in a packing of polyhedra where force anisotropy results mainly from the “facetted" particle shape.

REFERENCES

1. L. Rothenburg, and R. J. Bathurst, *Geotechnique* **39**, 601–614 (1989).
2. F. Radjai, M. Jean, J. Moreau, and S. Roux, *Phys. Rev. Letter* **77**, 274–277 (1996).
3. S. N. Coppersmith, C. Liu, S. Majumdar, O. Narayan, and T. A. Witten, *Phys. Rev. E* **53**, 4673–4685 (1996).
4. D. M. Mueth, H. M. Jaeger, and S. R. Nagel, *Phys. Rev. E.* **57**, 3164–3169 (1998).
5. L. E. Silbert, G. S. Grest, and J. W. Landry, *Phys. Rev. E* **66**, 1–9 (2002).
6. T. S. Majmudar, and R. P. Behringer, *Nature* **435**, 1079–1082 (2005).
7. F. Radjai, D. E. Wolf, M. Jean, and J. Moreau, *Phys. Rev. Letter* **80**, 61–64 (1998).
8. H. Ouadfel, and L. Rothenburg, *Mechanics of Materials* **33**, 201–221 (2001).
9. S. Antony, and M. Kuhn, *International Journal of Solids and Structures* **41**, 5863–5870 (2004).
10. E. Azéma, F. Radjai, R. Peyroux, and G. Saussine, *Phys. Rev. E* **76**, 011301 (2007).
11. M. Jean, *Computer Methods in Applied Mechanic and Engineering* **177**, 235–257 (1999).
12. J. Moreau, *Eur. J. Mech. A/Solids* **13**, 93–114 (1994).
13. F. Dubois, and M. Jean, “LMGC90 une plateforme de développement dédiée à la modélisation des problèmes d’intéraction.,” in *Actes du sixième colloque national en calcul des structures - CSMA-AFM-LMS* -, 2003, vol. 1, pp. 111–118.
14. J. J. Moreau, “Numerical Investigation of Shear Zones in Granular Materials,” in *Friction, Arching, Contact Dynamics*, edited by D. E. Wolf, and P. Grassberger, World Scientific, Singapore, 1997, pp. 233–247.
15. E. Azéma, F. Radjai, and G. Saussine, *Mechanics of Materials* **accepted** (2008).